Contrib Mineral Petrol (1985) 90:199–213

Contributions to Mineralogy and Petrology

Fe – Ti-Oxides in metamorphic basites from the Eastern Alps, Austria: a contribution to the formation of solid solutions of natural Fe – Ti-Oxide assemblages

E. Braun[1] **and M. Raith**[2]

[1] Institut für Mineralogie der Freien Universität, Takustraße 6, D-1000 Berlin, Federal Republic of Germany
[2] Mineralogisch-Petrologisches Institut und Museum der Universität, Poppelsdorfer Schloß, D-5300 Bonn, Federal Republic of Germany

Abstract. The development of Fe–Ti oxide assemblages in basic rocks from the Penninic series of the southern Venediger area, Austria, during polyphase Alpine metamorphism has been studied. Textural and compositional relations indicate thorough reequilibration of the opaque mineral assemblages during late Barrovian metamorphism at essentially static conditions of lower amphibolite to greenschist facies. In contrast, silicate mineralogy of the preceeding blueschist to eclogite facies metamorphism might still be preserved to a large extent.

Chemical adjustment of the Fe–Ti oxide minerals to decreasing $P-T$ conditions is characterized by (1) formation of complex intergrowths of ilmenite and hematite solid solutions ($<550°$ C), (2) the decomposition of hemo-ilmenite$_1$ to ferrianilmenite$_2$ + magnetite + rutile and of ilmeno-hematite$_1$ to titanhematite$_2$ + rutile ± magnetite ($<450°$ C), and (3) low-grade oxidation of ferrianilmenite$_2$ to magnetite + hematite-rutile intergrowths or hematite + rutile and of titanhematite$_2$ to hematite-rutile intergrowths ($\leqq 400°$ C). Chemical equilibrium is suggested by the regular partitioning of Cr, V, Mg and Mn between coexisting hemo-ilmenite, ilmeno-hematite, and magnetite. The hematite-ilmenite miscibility gap has been delimited on the basis of the bulk compositions of the exsolved phases and the temperature estimates obtained from Fe–Ti oxide thermometry.

Introduction

The composition of iron-bearing silicates in metamorphic rocks is related to the oxide ore assemblage because they are part of the complex oxide buffer system under closed system conditions (Chinner 1960; Annersten 1968). The temperatures and oxygen fugacities of equilibrated metamorphic oxide assemblages can be determined from the experimentally calibrated oxygen barometers and thermometers (Buddington and Lindsley 1964; Powell and Powell 1977). However, since natural Fe–Ti oxides usually contain significant amounts of Mg, Mn, Cr, V and Al (Carmichael 1967; Wass 1973; Braun 1974), the experimentally derived $T-fO_2$ equilibria for the pure $FeO-Fe_2O_3-TiO_2$ system can only be applied approximately (Powell and Powell 1977). Another complication in natural assemblages is the effect of the composition of the intergranular fluid phase (H_2O, CO_2, S_2, N_2 etc.) on the redox equilibria. In addition, the subsolidus reactions in silicate and oxide solid solutions have different rates. As a result in silicate assemblages, which are slower to re-equilibrate, mineral compositions generally reflect the thermal peak of metamorphism, while in Fe–Ti oxides, in which re-equilibration is able to occur at much lower temperatures (cf. Rollinson 1980), mineral compositions record retrograde temperatures. The present paper investigates the subsolidus miscibility of natural Fe–Ti oxides by studying a metamorphic rock series whose tectonic and metamorphic evolution is well-known from silicate mineral equilibria.

Geologic setting

The metabasites studied here are taken from a north-south profile through the Penninic series in the southern Venediger area (Austria). Detailed discussions of the tectonic structure, petrology, and metamorphic development of the rocks, with emphasis placed on the metabasites, can be found in Abraham et al. (1974), Raith et al. (1977, 1980), Miller (1974, 1977) and Holland (1977).

The metabasites range from tholeiitic to alkali-basaltic in composition (Raith et al. 1977) and appear in two different tectonic units (Fig. 1):

(1) The northern lower unit (Eclogite series) consists of a thin Mesozoic series of calc-mica schists and quartz rich garnet-mica schists (commonly containing graphite) with intercalations of numerous eclogitic and glaucophanitic metabasites (Raith et al. 1980). The base of the Eclogite series forms a thin Triassic series of marbles, quartzites and non-carbonate mica schists.

(2) The southern adjoining upper unit (Glockner nappe), which is separated from the lower unit by a prominent thrust plane, is much thicker and developed in typical Glockner facies. The Mesozoic Bündner schist series contains a thick succession of calc-phyllites, phyllites, and calc-mica schists, intercalated with chlorite schists, prasinites, and amphibolitic metabasites. These rocks overlie a thin unit of Triassic rocks that are chiefly carbonates, and a lamella of Paleozoic mica schists and albite porphyroblastic gneisses.

Two different metamorphic phases of mineral growth can be recognized in the metabasites which are part of a continuous metamorphic event (Raith et al. 1980; Holland 1979b). During the first eoalpine $>P/T$ metamorphism (90–60 m.y.) the basites of the Glockner nappe recrystallized from top to bottom progressively to chlorite schists,

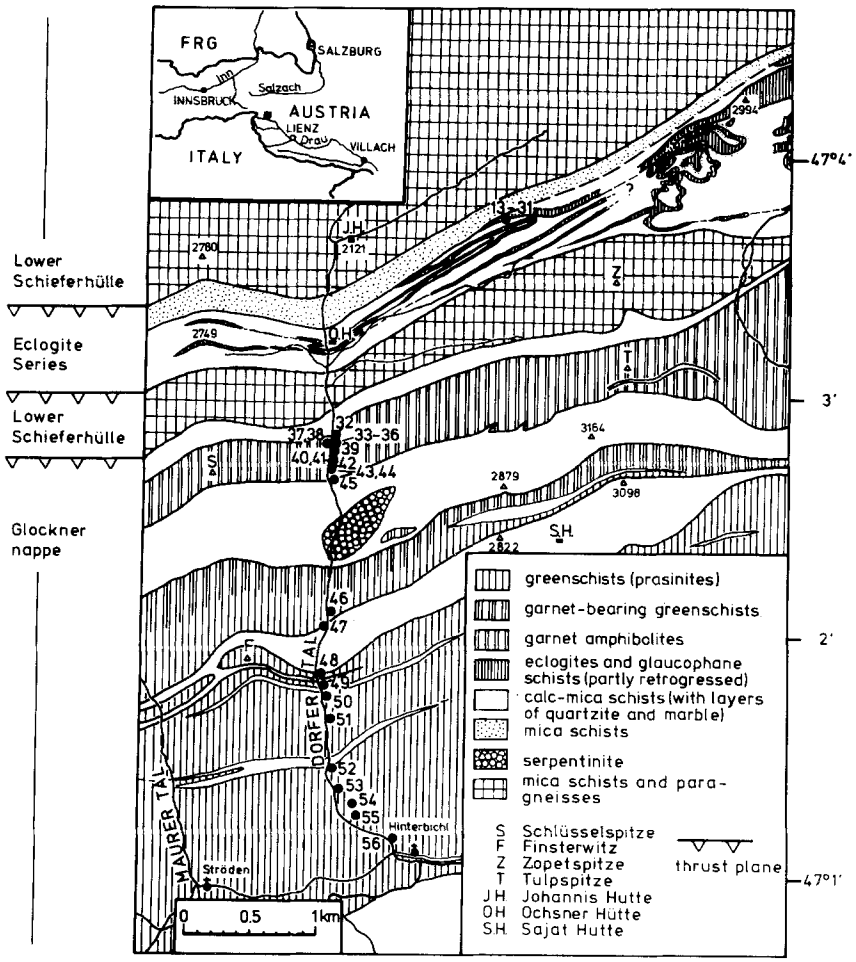

Fig. 1. Geological map of the southern Venedier area (according to Raith et al. 1980). Numbers give sample localities in the Dorfer valley profile

lawsonite- and glaucophanebearing schists ($P-T$ conditions: 350–400° C/4–6 kbars; Raith et al. 1980). The eclogitic and glaucophanitic metabasites of the Eclogite series were formed at markedly higher $P-T$ conditions (450–550° C/8–14 kbars: Miller 1977; Spiering 1979 resp. 620° C/17–22 kbars: Holland 1979a).

The eoalpine phase of metamorphism outlasted the formation of the nappe structure of the Penninic series. Recrystallization of eclogite rocks under static conditions and local transformation to glaucophane schists characterizes this postkinematic stage. At the end of this stage the intensely folded and sheared series shows prograde high-pressure metamorphism from the top to the bottom of the section.

The subsequent early Tertiary metamorphic phase (60–40 m.y. ago), probably occurred at slightly higher temperatures and lower pressures, causing a further overprint of the Penninic series. The lawsonite- and glaucophane-garnet-bearing metabasites of the Glockner nappe recrystallized under greenschist facies conditions (400° C/4 kbars) to prasinites. The eclogites and glaucophane schists of the Eclogite series locally recrystallized to amphibolitic and prasinitic metabasites at lower amphibolite to greenschist facies conditions (550° C/5 kbars).

Opaque mineral assemblages

Prasinites

Textural features suggest that the opaque mineral assemblages recrystallized at greenschist facies conditions (Table 1). The assemblages pyrite + chalcopyrite and magnetite + hematite are widespread. Less commonly magnetite + hematite + rutile, hematite or magnetite are found. All these assemblages occur in layers and may alternate on a rather small scale. Rock types with abundant sulfides commonly contain minor amounts of magnetite and sphene. Ferrianilmenite is observed solely as relics in association with pyrite and chalcopyrite in one prasinitic metabasite (sample 56). Magnetite is the only opaque oxide mineral found in contact with sulfide minerals, and replacement of Fe–Ti oxides by sulfidization reactions has not been observed. In highly oxidized prasinites and chlorite schists hematite + rutile are preserved in the cores of Fe^{3+}-rich epidote grains (e.g. samples 50a, b and 49a, b) as relics from an earlier metamorphic stage.

The regional variation of opaque assemblages in the prasinites is essentially the result of local differences in the oxygen and sulphur fugacities and probably reflects the primary redox-changes of the source rock (Thompson 1972). The phase relationships between the Fe–Ti oxides correspond with those of the lower greenschist facies (Fig. 2; compare also Rumble III 1976).

Magnetite in the prasinitic rocks is most commonly equant and euhedral. An additional late skeletal type (15–250 μm across) is also observed. In reflected light magnetite is optically homogeneous without discernable zoning or exsolution. Incipient martitization is present around grain boundaries and along cleavage planes. Magnetite is a late postkinematic product, and it commonly encloses and surrounds silicates, but it also may enclose sulfides, hematite, or traces of ilmenite.

Titanhematite and rare Fe^{3+}-free ilmenite occur in the centers of coronar aggregates of sphene. These hematites show acicular rutile exsolution textures (1–1.5 μm in length), which are oriented parallel

Table 1. Opaque mineral associations of the metabasites

Sample	Rock type	Opaque mineral assemblages	
		opaque oxides[a]	sulfides
56	prasinite	magnetite, ilmenite, rutile, sphene	chalcopyrite, pyrite
55	prasinite	magnetite, sphene	chalcopyrite, pyrite
54a, b	prasinite	magnetite, ilmeno-hematite, sphene	chalcopyrite, pyrite
50a, b	prasinite	magnetite, ilmeno-hematite, rutile, sphene	chalcopyrite, covellite
49a, b	prasinite	magnetite, ilmeno-hematite, rutile, sphene	–
44	garnet amphibolite	ilmeno-hematite, hemo-ilmenite, rutile, sphene	–
43	garnet amphibolite	magnetite, hemo-ilmenite, rutile	–
42a, b	garnet amphibolite	magnetite, hemo-ilmenite, ilmeno-hematite, rutile	chalcopyrite, pyrite
41	garnet amphibolite	hemo-ilmenite, rutile	chalcopyrite, pyrite
40	garnet amphibolite	magnetite, ilmeno-hematite, hemo-ilmenite, rutile	–
39	garnet amphibolite	hemo-ilmenite, ilmeno-hematite, rutile	pyrrhotite
38	garnet amphibolite	hemo-ilmenite, rutile, sphene	chalcopyrite, pyrite, pyrrhotite
37	garnet amphibolite	magnetite, hemo-ilmenite, rutile, sphene	chalcopyrite, pyrite, pyrrhotite
36	garnet amphibolite	magnetite, hemo-ilmenite, ilmeno-hematite, rutile	pyrite, pyrrhotite
35	garnet amphibolite	magnetite, hemo-ilmenite, ilmeno-hematite, rutile	chalcopyrite, pyrrhotite
34	garnet amphibolite	magnetite, hemo-ilmenite, ilmeno-hematite, rutile, sphene	pyrrhotite
33	garnet amphibolite	magnetite, hemo-ilmenite, ilmeno-hematite, rutile	chalcopyrite
32	garnet amphibolite	hemo-ilmenite, hematite, rutile, sphene	chalcopyrite, pyrite, pyrrhotite
31	eclogite (glauc.)*	hemo-ilmenite, ilmeno-hematite, rutile	pyrite
24	eclogite (diaph.)**	magnetite, ilmeno-hematite, rutile, sphene	–
23	eclogite (glauc.)	magnetite, ilmeno-hematite, rutile	–
22	eclogite (diaph.)	magnetite, ilmeno-hematite, hemo-ilmenite, rutile	–
21	eclogite (glauc.)	magnetite, hemo-ilmenite, rutile	pyrrhotite
20	eclogite (diaph.)	hemo-ilmenite, rutile, sphene	chalcopyrite, pyrrhotite
19	eclogite (diaph.)	magnetite, ilmeno-hematite, rutile	–
18	eclogite (diaph.)	magnetite, ilmeno-hematite, rutile	–
17	eclogite (glauc.)	magnetite, hemo-ilmenite, ilmeno-hematite, rutile, sphene	pyrite

[a] Terminology of the rhombohedral Fe–Ti oxides as far as oxidation and exsolution products are concerned, after Buddington et al. (1963) and Anderson (1968): hemo-ilmenite = intergrowth of titan-hematite and a ferrian-ilmenite host; ilmeno-hematite = intergrowth of ferrian-ilmenite and a titan-hematite host; * glaucophanitic eclogite; ** diaphthoritic eclogite

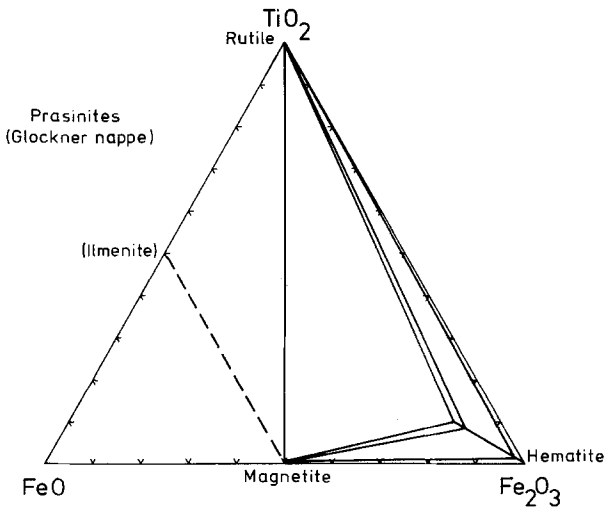

Fig. 2. Fe–Ti oxide parageneses of prasinitic metabasites: rutile + magnetite + hematite (samples 50a, b; 49a, b), magnetite + hematite (54a, b), magnetite + ilmenite (56) and magnetite (55)

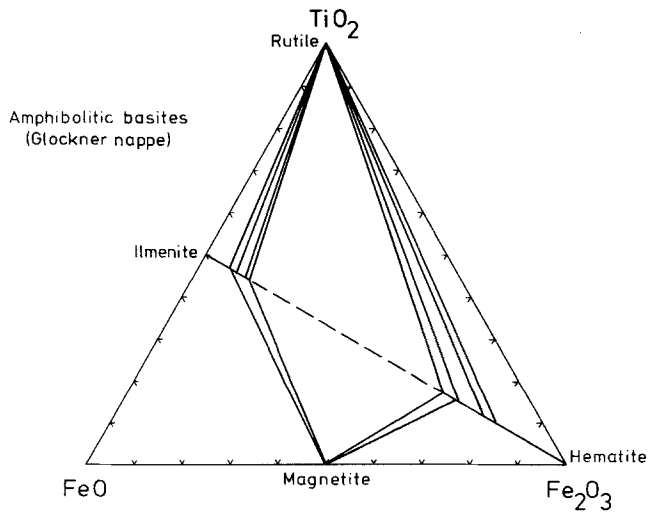

Fig. 3. Phase relations of coexisting Fe–Ti oxides in amphibolitic metabasites. Parageneses studied are: rutile + hematite + ilmenite (samples 44; 39; 32), magnetite + ilmenite + hematite (42a, b; 40; 36; 35; 34; 33), rutile + ilmenite (41; 38) and magnetite + ilmenite (43; 37)

$(10\bar{1}1)$ of the host crystal. In addition subhedral hematite laths are distributed through the rock and represent part of the equilibrated opaque assemblage. These hematites also exhibit rutile needles (15–20 μm in length and 1–1.5 μm in width), which are mainly restricted to the cores of the grains. Postkinematic hematite idioblasts commonly occur in the proximity of sphene, enclosing hematite and rutile relics. This hematite-generation is characterized by optical homogeneity, by the absence of lamellar rutile exsolution, and by the rarity of inclusions. The tabular crystals are intimately intergrown with sphene without being replaced by it.

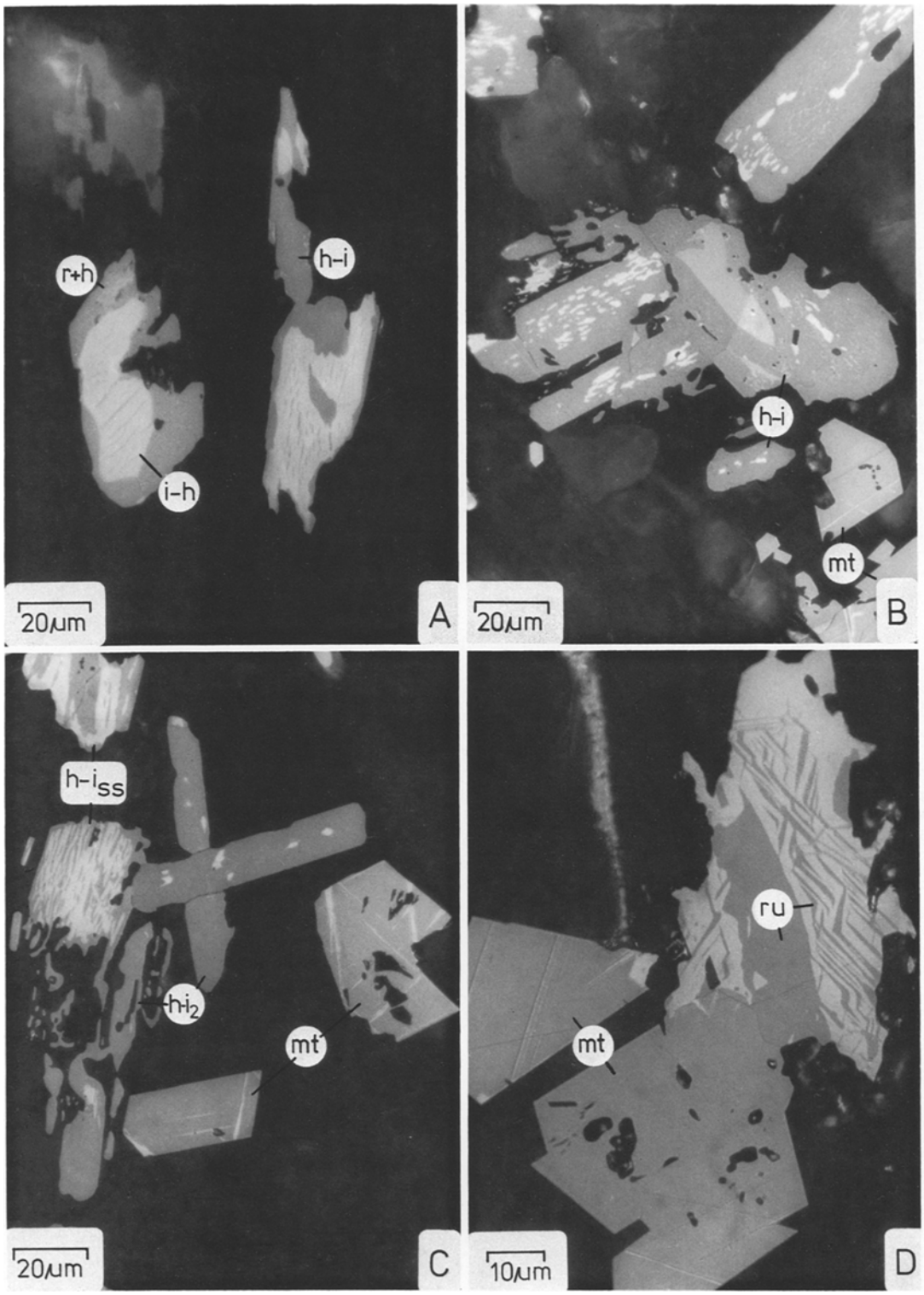

Fig. 4. Fe–Ti-oxides in amphibolitic and eclogitic metabasites. **A** Extensive high temperature migration forms subhedral hemo-ilmenite (*h–i*) with tiny hematite exsolutions in the form of strings of pearls. Ilmeno-hematite (*i–h*) shows a set of well oriented ilmenite lamellae. The speckled area in the upper part of the ilmenite grain (*left side*) is due to diaphthoritic oxidation and consists of rutile + hematite (*r + h*); garnet amphibolite 33. **B** Ilmenite (*h–i*) exsolves a lenticular and a second string-shaped (3.5–1 µm) ilmeno-hematite generation. Subhedral magnetite (*mt*) exhibits thin martite lamellae //(111) of the spinel; eclogite 17. **C** Anhedral ilmenite-hematite solid solutions (h–i_{ss}) with sandwich-like structure are replaced by a secondary hematite-poor idiomorphic ilmenite (h–i_2), in part with skeletal growth. Idiomorphic, martitized magnetite (*mt*) coexists with these ilmenite blasts; eclogite 17. **D** Diaphthoritic generation of euhedral magnetite (*mt*), weakly martitized, coexists with hematite exsolving rutile. Rutile (*ru*) exsolutions consist of coarse rutile laths, being in direct contact to magnetite and thin lamellae, oriented //$(10\bar{1}1)$ of hematite; eclogite 19

Rutile is always accompanied by traces of hematite and it occurs as rare inclusions in sphene and in the Ti-rich cores of large hematite idioblasts. In both cases it represents the oxidation product of an originally Ti-rich ilmeno-hematite.

Garnet-amphibolites

The typical opaque mineral assemblages of the garnet-bearing amphibolitic and prasinitic rock types are (Fig. 3):
hemo-ilmenite + ilmeno-hematite + rutile,
hemo-ilmenite + ilmeno-hematite + magnetite ± rutile,
magnetite + ilmenite, rutile + ilmenite, and rutile + hematite.

In addition, chalcopyrite, pyrrhotite, and pyrite are present in varying amounts (Table 1). As in the prasinites, the euhedral sulfides from the garnet amphibolites are not intergrown with the opaque oxides. Incipient limonitization of pyrite is commonly observed.

Hemo-ilmenite primarily forms rims around spherical hematite grains. Subhedral ilmenite, which may be enclosed by late almandine-rich garnet, generally shows three types of hematite exsolution:
(a) a roughly spotted or spindle shaped ilmeno-hematite generation attaining volumes of equal size if compared to the ilmenite host (Fig. 4a);
(b) a finely spotted to lenticular hematite with maximum diameter of 5–20 μm, which is mainly exsolved in the marginal areas of the ilmenite grains;
(c) and very fine-grained textured hematite having the form of "strings of pearls" measuring 1–1.5 μm.

A typical texture in the garnet-bearing metabasites is graphic intergrowths of ilmenite and silicates which grow epitactically on the octahedral faces of magnetite crystals. These ilmenites often exsolve large amounts of anhedral hematite at the margins of the grains. Because it is a late oxidation product, this hematite is intergrown with acicular rutile. Depending on the degree of oxidation, ilmenite can be observed with coarse interlayered lamellae or irregularly distributed spots of rutile. Along with the anhedral hematite occurring at the margins of ilmenite, these complex intergrowths represent different stages of ilmenite alteration to hematite and rutile.

Late diaphthoritic oxidation leads to irregular speckling of ilmenite, caused by fine-grained intergrowth of rutile and Ti-hematite. These 2–5 μm large spottedly arranged oxidation products even may completely replace the ilmenite host.

Ilmeno-hematite occurs both in the sandwich-type intergrowths with hemo-ilmenite described above and as independent subhedral grains in the silicate matrix. The exsolution textures of both ilmeno-hematite types are identical. Ilmenite is exsolved in two generations:
(a) as spotted, commonly platy to string shaped bodies, 5–35 μm in length;
(b) as very fine lamellae, 2–1 μm thick, interstratifying the hematite host subparallel to (0001).

Highly oxidized rocks contain hematite with acicular shaped rutile exsolutions usually oriented parallel to $(10\bar{1}1)$. Flames or anhedral grains of rutile are also commonly observed. Oxidation products of former ilmeno-hematite are hematite-rutile sandwich-structures. The hematite part of these structures shows rutile layers, and the rutile contains hematite lamellae. A late hematite generation that is similar to the hematite of the prasinites is commonly phacoidally or tabular shaped, optically homogeneous, and free of inclusions.

In addition to intergrowths with ilmenite and hematite, subhedral to rounded *rutile* occurs as an independent phase in the silicate matrix.

Euhedral *magnetite* appears in the chloritized margins of almandine-rich garnets where it was formed as a break-down product. These 25–50 μm magnetite idioblasts are easily distinguished from the coarser grained (120–150 μm) euhedral magnetite of the matrix. Textural relations indicate that this second magnetite generation is of the same age as the ilmenite-silicate symplectites discussed above. Tabular hemo-ilmenite can be found in contact with magnetite. The magnetites are microscopically homogeneous, except for fine-grained silicate inclusions. Rarely, incipient martitization at grain boundaries is observed.

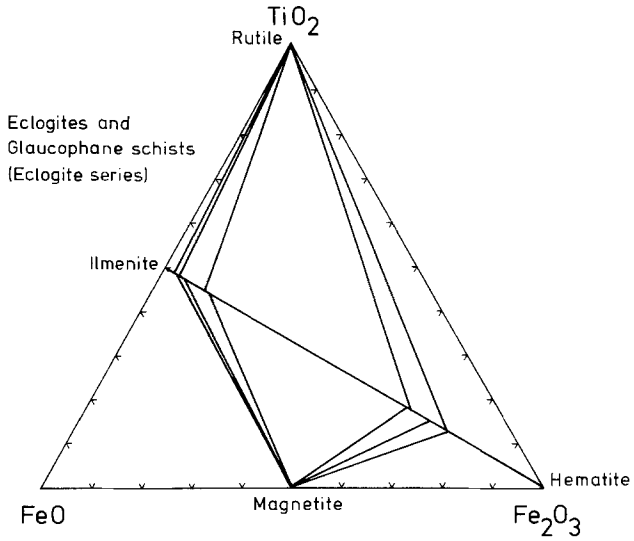

Fig. 5. Phase relations of coexisting Fe–Ti oxides in eclogites and glaucophane schists. Mineral assemblages of the eclogitic stage: rutile + ilmenite + hematite (samples 31; 17), magnetite + ilmenite (21), ilmenite + rutile (31; 21; 20) and ilmenite + hematite + magnetite (22; 17)

Eclogites

Rutile is the dominant opaque mineral in the majority of the eclogites and glaucophane schists. In addition, hemo-ilmenite, ilmeno-hematite, and the sulfides pyrrhotite, pyrite, and chalcopyrite may be present depending on the prevailing redox conditions. In the moderately retrogressed rock types the following Fe–Ti oxide assemblages are encountered (Fig. 5):

rutile + hematite + ilmenite, ilmenite + rutile, ilmenite + magnetite and ilmenite + hematite + magnetite.

The opaque mineral assemblages of the strongly retrogressed metabasites show a higher degree of oxidation:

hematite + magnetite + rutile relics, rutile + hematite and hematite + magnetite.

In the altered eclogites and glaucophane schists rutile and ilmenite are largely replaced by sphene.

Rutile appears as an excess phase in all assemblages. The euhedral iron-rich rutile is almost free of inclusions and unzoned. Sporadic spots of ilmenite can be seen along the grain boundaries. Extensive intergrowth with ilmenite or ilmeno-hematite is only rarely found. These textural relations are strongly suggestive of replacement processes. In retrogressed eclogites, rutile becomes unstable and shows extensive replacement by ilmenite and hematite, whereby the external outlines of the rutile grains are fairly well preserved. Apart from these partial pseudomorphs, extremely altered eclogites contain a second rutile generation which along with hematite replaces ilmenite. Two samples show that these ilmenite oxidation products can be progressively replaced by sphene, which leaves an eclogitic mineral assemblage essentially free of rutile. This phenomenon has already been described in the prasinitic rocks.

The *ilmenite* in the eclogites, as in the amphibolite assemblages, is characterized by two generations of hematite exsolution

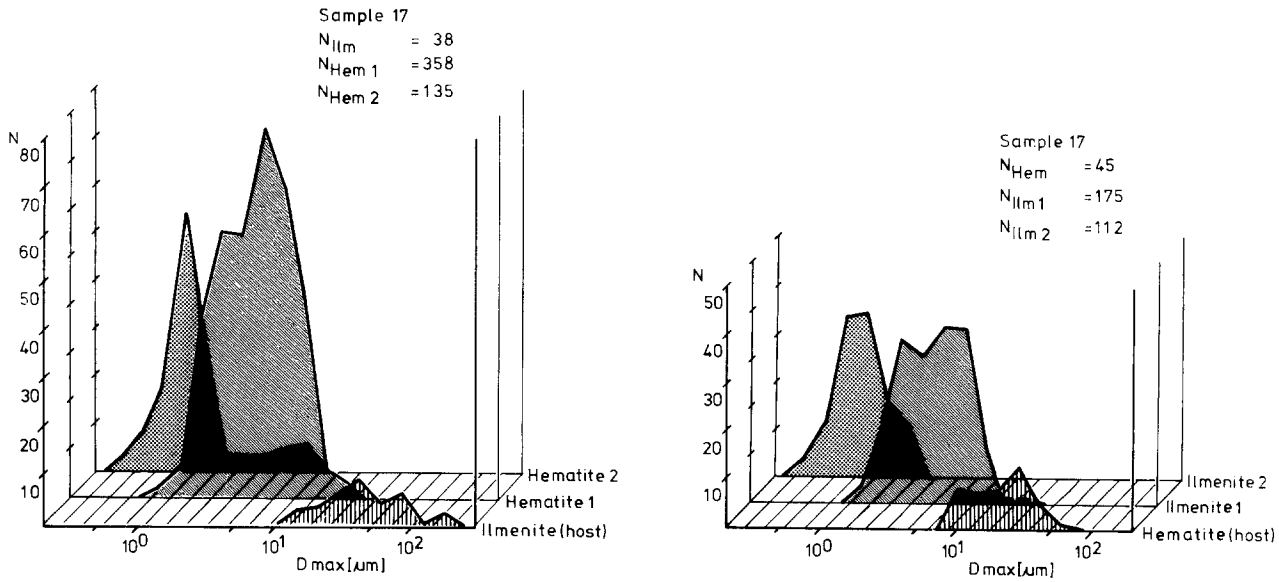

Fig. 6. Characteristic grain size distributions of coexisting ilmenites and hematites. The planimetric analyses respectively include host-crystals and two generations of exsolution. Investigation were performed on 38 ilmenite and 45 hematite grains of the eclogite sample 17; 100 × oil immersion objective

Table 2. Analytical procedure, detectability limits and precision for major, minor and trace elements

Elements	Major elements		Minor and trace elements									
	Fe	Ti	Ti	V	Al	Mn	Mg	V	Mn	Ni	Cr	Zn
Wt.% in standard	46.54	45.70	1.60	1.10	6.23	4.77	0.31	0.20	0.17	0.14	0.10	0.16
Oxides	FeO[a]	TiO_2	TiO_2	V_2O_3	Al_2O_3	MnO	MgO	V_2O_3	MnO	NiO	Cr_2O_3	ZnO
Standards[b]	1	1	2	2	3	1	1	4	4	4	5	2
Wt.% in Fe–Ti phases	46–93	10–50	0–9	0.5–1.4	0–1.4	1–4	0–0.7	0–0.4	0–0.7	0–0.1	0–0.04	0–0.4
Detectability limits[c]	–	–	0.02	0.02	0.02	0.06	0.05	0.02	0.06	0.02	0.02	0.04
1σ (%)	0.5	1.0	1.3	1.4	2.2	1.0	3.1	2.5	8.9	7.8	4.0	9.3

[a] Total iron as FeO
[b] Mineral standards obtained from E. Jarosewich, Smithsonian Institution, Washington: 1-Ilmenite NMNH 96189; 2-Chromite 53-IN-8; 3-Chromite GS-2; 4-Chromite 55-G-17; 5-Augite, Kakanui
[c] Detectability limits calculated according to Kaiser (1965)

(Fig. 4b). The composite ilmenite grains exhibit hematite lenses grading progressively into sandwich laths. This hematite generation exsolves elongated discs of ilmenite. SEM images of exsolved hematite which is at the limit of optical resolution, show that it forms string-like intertwined exsolution clusters. Areas of from 2 to 10 µm in the ilmenite host which are adjacent to first generation ilmeno-hematite lamellae are free of optically recognizable hematite exsolutions. The same holds when the smaller ilmeno-hematite spots of the second generation accumulate in marginal regions of the ilmenite grains (Fig. 6).

A characteristic oxidation product of primary hemo-ilmenite is euhedral lath-shaped ilmenite. This second generation of ilmenite formed by the oxidation reaction: hemo-ilmenite$_1$ + O_2 = hemo-ilmenite$_2$ + ilmeno-hematite$_2$, whereby minute drop-like hematite is exsolved (Fig. 4c). The ilmeno-hematite$_2$ itself exhibits only few coarse-layered ilmenite exsolutions, an intimately disseminated ilmenite phase is not traceable. Advanced diaphthoritic oxidation ultimately causes the already described speckled ilmenite, i.e. its transformation to hematite and rutile.

Ilmeno-hematite exsolves coarse lath-shaped ilmenite and a second generation of minute drop-like ilmenite. These complex intergrowths are rimmed by ilmenite which is essentially free of hematite exsolutions and frequently in direct contact with independent ilmenite idioblasts. As a result of complete oxidation of ilmeno-hematite and possibly also of hemo-ilmenite subhedral hematite crystals with a laminated rutile intergrowth are formed.

Magnetite with incipient martitization typically occurs in retrogressed glaucophane schists. The martite lamellae are predominantly oriented parallel to the (111) planes of the spinel (Fig. 4c). Except for minor silicate inclusions, the euhedral magnetite crystals are optically homogeneous and always free of recognizable zoning. A late generation of subhedral or skeletal magnetite replaces ilmenite-rutile intergrowths and hemo-ilmenite. It coexists with hematite and rutile in the opaque mineral assemblages of diaphthoritic samples. Furthermore, a second generation of fine-grained euhedral magnetite is formed as break-down product of the garnets. This

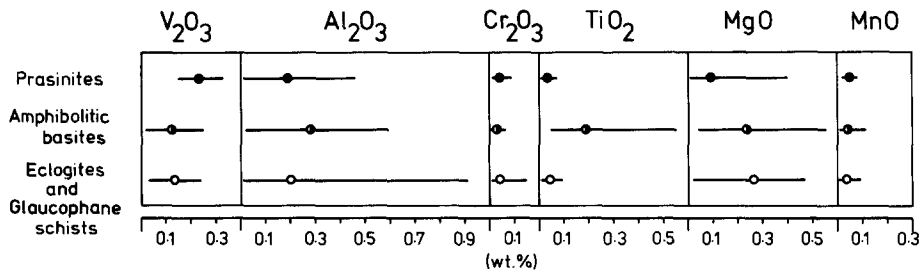

Fig. 7. Minor element concentrations of magnetites. Average values and maximum variation of oxides are plotted for eclogitic (*open circles*), amphibolitic (*half-filled circles*) and prasinitic metabasites (*filled circles*)

homogeneous magnetite is frequently observed coexisting with secondary hematite.

Analytical techniques and recalculation of microprobe analyses

Wave length dispersive analyses of the Fe–Ti oxides in 31 metabasite samples were done with the JEOL 3A microprobe at the Mineralogisch-Petrographisches Institut, TU Clausthal and the ARL-SEMQ microprobe at the Institut für Mineralogie of the FU Berlin. Operating conditions were: 20 kV (accelerating voltage) and 35–40 nA sample current. Natural minerals with structures and compositions close to those of the Fe–Ti phases (Table 2) were used as standards. The overlap effect of the TiK_β line on the VK_α line was checked on low-V chromite standards with variable Ti concentrations using a LiF crystal with a $\Delta\lambda$ of 0.0091 Å. Data reduction was done using the EMPADR VII computer program (Rucklidge and Gasparrini 1969) and the Bence-Albee correction procedure (Bence and Albee 1968).

Generally, three to six mineral grains or aggregates were analyzed per specimen depending on their microanalytical suitability. Each mineral analysis represented in the Tables is an average of 4–6 individual analyses. Compositional homogeneous magnetite and rutile were analyzed with a finely focussed electron beam. A larger diameter electron beam was used to analyze ilmenite and hematite in an attempt to compensate for complex intergrowths. The finest-grained ilmenite or hematite exsolutions of the second generation with a maximum diameter of 1–3 μm could not be measured separately and was analyzed together with its host mineral. The bulk compositions of the exsolved rhombohedral phases were analyzed with an analysis-spot of 20–30 μm in diameter as described by Rumble III (1973) and recently by Thy (1982). The proportion of the exsolved phases in individual Fe–Ti oxide grains were planimetrically analyzed and the average analyses of the rhombohedral phases used to calculate the bulk compositions.

Ilmenite and hematite structural formulae are assumed to be stoichiometric and calculated from the analyses on the basis of 4 cations with as much Fe^{2+} converted to Fe^{3+} as is necessary to bring the oxygen total to 6. In the resulting structural formulae Fe^{2+} and Ni^{2+} are combined and represent the ilmenite component. Mg and Mn represent the geikielite and pyrophanite components respectively. One half the combined Fe^{3+}, V^{3+}, Cr^{3+}, and Al^{3+} represents the hematite component.

The magnetite analyses are recalculated to structural formulae on the basis of 24 cations. The calculation of ideal spinel end members can be based on different assumptions (cf. Bowles 1977a and b). The calculation scheme used here is a modified version of the recasting procedure proposed by Morse (1980), which has been successfully adopted for T–fO_2 evaluations of magmatic Fe–Ti oxide parageneses.

Chemistry of the Fe–Ti oxides

Magnetite

The magnetites are both optically and chemically homogeneous (Table 3). They have low and constant MnO- and Cr_2O_3 contents of about 0.1 wt.% (Fig. 7). In the transition from prasinites to amphibolitic eclogites and glaucophane schists V_2O_3 of the magnetites shows a perceptible decrease from 0.25 to 0.1 wt.%, while Al_2O_3 and MgO show slight increases. Contents of 0.2 wt.% Al_2O_3 and 0.2 wt.% MgO in magnetite from the prasinite samples increase to 0.9 and 0.3 respectively in the eclogitic metabasites. TiO_2 is generally low (<0.1 wt.%) but attains a maximum content of 0.55 wt.% in the amphibolite sample 34. The low and varying contents of the corresponding spinel constituents (ulvöspinel and aluminate spinels, cf. Table 3) are comparable to magnetites from metamorphic rocks of similar grade studied by Buddington and Lindsley (1963), Abdullah and Atherton (1964), Westra (1970), Mielke and Schreyer (1972) and Rumble (1976). The ulvöspinel component in the prasinites is only 0.1 mol.% and varies between 0.2 and 0.5 mol.% in the amphibolitic metabasites with the exception of sample 34, which has the highest ulvöspinel content (1.6 mol.%).

Ilmenite, hematite and rutile

The chemistry of the ilmenite and hematite phases is extremely complex because of the very fine-grained exsolution and intergrowth textures. Table 4 reports selected microprobe analyses of the coarse ilmenite and hematite phases in complex sandwhich-type intergrowths.

The Mn and Mg contents of the *ilmenites* show an apparent dependence on metamorphic grade (Fig. 8). In contrast to ilmenites from amphibolites those from eclogitic rocks are markedly enriched in $MgTiO_3$ (4–6 mol.%). This could be due to the much higher pressures of eclogite formation (20–14 kbars) favouring the introduction of the small cation Mg^{2+} into the ilmenite structure. The later generation ilmenites, which formed in altered eclogites at much lower pressures (<6 kbars), are essentially free of $MgTiO_3$. Instead, these ilmenites have higher contents of $MnTiO_3$ (up to 8.5 mol.%). The ilmenite phase exsolved in the coexisting hematite, in comparison, is poor in $MnTiO_3$, but like the ilmenite host crystals is characterized by rather high $MgTiO_3$ contents (Fig. 8). Ilmenite lamellae of prasinite hematites are almost pure $FeTiO_3$ phases.

The *hematites* are distinctly enriched in V_2O_3 and Cr_2O_3 when compared to the coexisting ilmenites (Table 4). This enrichment is independent of the metamorphic grade and is the result of similar ionic radii (Fe^{3+}:0.63 Å, V^{3+}:0.72 Å, Cr^{3+}:0.70 Å, cf. Schuiling and Feenstra 1980; ionic radii by Whittacker and Muntus 1970). Mn in contrast to Cr has a siderophilic character thus favouring a compound with Mn^{2+} (pyrophanite component). This is confirmed by experiments on Fe–Ti oxides (Rumble III 1973;

Table 3. Microprobe analyses, structural formulae and molecular spinel components of magnetites

Rock type	Prasinites						Amphibolitic basites								Eclogites and glaucophane schists						
Sample	55	54b	54a	50b	50a	49a	43	42a	40	37	36	35	34	33	24	23	22	21	19	18	17
N^a	3	3	6	3	3	3	3	4	3	4	3	3	3	3	3	3	6	4	5	3	4
SiO_2	0.00	0.00	0.00	0.00	0.00	0.00	0.00	0.00	0.00	0.00	0.00	0.00	0.00	0.00	0.00	0.00	0.00	0.00	0.00	0.00	0.00
TiO_2	0.03	0.01	0.03	0.02	0.03	0.02	0.06	0.06	0.12	0.16	0.06	0.18	0.55	0.07	0.03	0.04	0.03	0.02	0.04	0.03	0.07
Al_2O_3	0.18	0.19	0.27	0.07	0.24	0.10	0.07	0.08	0.24	0.23	0.41	0.32	0.51	0.09	0.09	0.39	0.11	0.15	0.18	0.09	0.33
Cr_2O_3	0.05	0.02	0.06	0.01	0.06	0.01	0.00	0.08	0.03	0.01	0.02	0.01	0.02	0.03	0.08	0.03	0.03	0.06	0.01	0.04	0.05
V_2O_3	0.17	0.17	0.26	0.31	0.27	0.18	0.17	0.26	0.13	0.10	0.04	0.04	0.18	0.09	0.14	0.02	0.06	0.28	0.17	0.17	0.17
FeO^b	91.40	92.51	91.73	89.55	90.68	91.73	93.13	92.62	92.89	91.91	93.65	93.22	92.73	91.54	91.01	91.51	91.37	91.35	91.43	92.28	92.33
MnO	0.03	0.04	0.04	0.06	0.06	0.06	0.01	0.02	0.05	0.01	0.05	0.04	0.06	0.03	0.06	0.02	0.00	0.01	0.03	0.04	0.07
MgO	0.16	0.23	0.15	0.02	0.00	0.00	0.40	0.01	0.14	0.16	0.15	0.09	0.11	0.06	0.36	0.26	0.41	0.07	0.11	0.17	0.25
NiO	0.03	0.04	0.03	0.02	0.04	0.08	0.02	0.08	0.03	0.01	0.01	0.01	0.02	0.08	0.01	0.03	0.07	0.04	0.06	0.06	0.05
CaO	0.11	0.07	0.12	0.22	0.07	0.17	0.02	0.12	0.04	0.18	0.20	0.21	0.16	0.07	0.13	0.05	0.22	0.09	0.11	0.18	0.16
ZnO	0.01	0.01	0.01	0.01	0.01	0.00	0.00	0.00	0.01	0.01	0.01	0.00	0.00	0.01	0.02	0.01	0.01	0.00	0.01	0.01	0.00
Total	92.17	93.29	92.70	90.29	91.46	92.35	93.88	93.33	93.68	92.78	94.60	94.12	94.34	92.07	91.93	92.36	92.31	92.07	92.15	93.07	93.48
structural formulae based on 24 cations and 32 oxygens																					
Mn	0.01	0.01	0.01	0.02	0.02	0.02	0.00	0.00	0.01	0.00	0.01	0.01	0.01	0.01	0.02	0.00	0.00	0.00	0.01	0.01	0.02
Mg	0.07	0.10	0.07	0.01	0.00	0.00	0.18	0.00	0.06	0.07	0.07	0.04	0.05	0.03	0.17	0.12	0.19	0.03	0.05	0.08	0.11
Ni	0.01	0.01	0.01	0.01	0.01	0.02	0.00	0.02	0.01	0.00	0.00	0.00	0.00	0.02	0.00	0.01	0.02	0.01	0.01	0.01	0.01
Ca	0.04	0.02	0.04	0.07	0.02	0.06	0.01	0.04	0.01	0.06	0.06	0.07	0.05	0.02	0.04	0.02	0.07	0.03	0.04	0.06	0.05
Zn	0.00	0.00	0.00	0.00	0.00	0.00	0.00	0.00	0.00	0.00	0.00	0.00	0.00	0.00	0.00	0.00	0.00	0.00	0.00	0.00	0.00
Fe 2+	7.87	7.85	7.87	7.89	7.95	7.91	7.80	7.93	7.90	7.86	7.85	7.88	7.88	7.92	7.77	7.85	7.72	7.92	7.89	7.83	7.80
Al	0.07	0.07	0.10	0.03	0.09	0.04	0.02	0.03	0.09	0.08	0.15	0.11	0.18	0.03	0.03	0.14	0.04	0.05	0.07	0.03	0.12
Cr	0.01	0.00	0.01	0.00	0.01	0.00	0.00	0.02	0.01	0.00	0.00	0.00	0.00	0.01	0.02	0.01	0.01	0.01	0.00	0.01	0.01
V	0.04	0.04	0.06	0.08	0.07	0.04	0.04	0.06	0.03	0.02	0.01	0.01	0.04	0.02	0.03	0.00	0.01	0.07	0.04	0.04	0.04
Ti	0.01	0.00	0.01	0.01	0.01	0.00	0.01	0.01	0.03	0.04	0.01	0.04	0.12	0.02	0.01	0.01	0.01	0.00	0.01	0.01	0.02
Si	0.00	0.00	0.00	0.00	0.00	0.00	0.00	0.00	0.00	0.00	0.00	0.00	0.00	0.00	0.00	0.00	0.00	0.03	0.00	0.00	0.00
Fe 3+	15.87	15.88	15.82	15.89	15.82	15.91	15.92	15.87	15.85	15.85	15.83	15.83	15.64	15.92	15.90	15.84	15.93	15.83	15.88	15.91	15.81
$MgAl_2O_4{}^c$	0.41	0.43	0.61	0.12	0.00	0.00	0.16	0.06	0.54	0.52	0.85	0.51	0.62	0.21	0.21	0.89	0.25	0.34	0.41	0.20	0.74
$FeAl_2O_4$	0.00	0.00	0.00	0.02	0.53	0.23	0.00	0.12	0.00	0.00	0.04	0.21	0.52	0.00	0.00	0.00	0.00	0.00	0.00	0.00	0.00
$ZnAl_2O_4$	0.00	0.00	0.00	0.03	0.03	0.00	0.00	0.00	0.00	0.00	0.03	0.00	0.00	0.03	0.03	0.03	0.03	0.00	0.03	0.03	0.03
Fe_2TiO_4	0.09	0.03	0.09	0.06	0.09	0.06	0.17	0.17	0.35	0.46	0.17	0.52	1.57	0.20	0.09	0.12	0.09	0.06	0.12	0.09	0.20
$FeCr_2O_4$	0.08	0.03	0.09	0.02	0.09	0.01	0.00	0.12	0.05	0.01	0.03	0.01	0.03	0.05	0.12	0.05	0.05	0.09	0.01	0.06	0.08
$MgFe_2O_4$	0.00	0.89	0.25	0.00	0.00	0.00	2.11	0.00	0.26	0.40	0.00	0.00	0.00	0.14	1.88	0.61	2.12	0.06	0.22	0.77	0.68
$NiFe_2O_4$	0.09	0.12	0.09	0.06	0.13	0.25	0.06	0.25	0.09	0.03	0.03	0.03	0.06	0.25	0.03	0.09	0.22	0.12	0.19	0.19	0.15
$MnFe_2O_4$	0.10	0.13	0.13	0.20	0.20	0.20	0.03	0.06	0.16	0.03	0.16	0.13	0.19	0.10	0.20	0.07	0.00	0.03	0.10	0.13	0.23
FeV_2O_4	0.26	0.26	0.40	0.49	0.42	0.28	0.26	0.40	0.20	0.15	0.06	0.06	0.27	0.14	0.22	0.03	0.09	0.44	0.26	0.26	0.26
Fe_3O_4	98.45	98.11	98.33	99.00	98.51	98.97	97.20	98.81	98.36	98.38	98.63	98.53	96.73	98.88	97.22	98.12	97.16	98.85	98.65	98.27	97.62
X Usp	0.09	0.03	0.09	0.06	0.09	0.06	0.18	0.17	0.35	0.47	0.17	0.52	1.60	0.21	0.09	0.12	0.09	0.06	0.12	0.09	0.21

[a] Number of analyzed magnetites

[b] Total iron as FeO

[c] The maximum error of molecular spinel components has been calculated from the standard deviation of the elements Fe, Ti, Mn, Mg, V and Cr and amounts to ± 0.5 mol.% Fe_3O_4, ± 0.06 mol.% Fe_2TiO_4, ± 0.16 mol.% $MgAl_2O_4$, ± 0.02 mol.% $MnFe_2O_4$, FeV_2O_4 and $FeCr_2O_4$

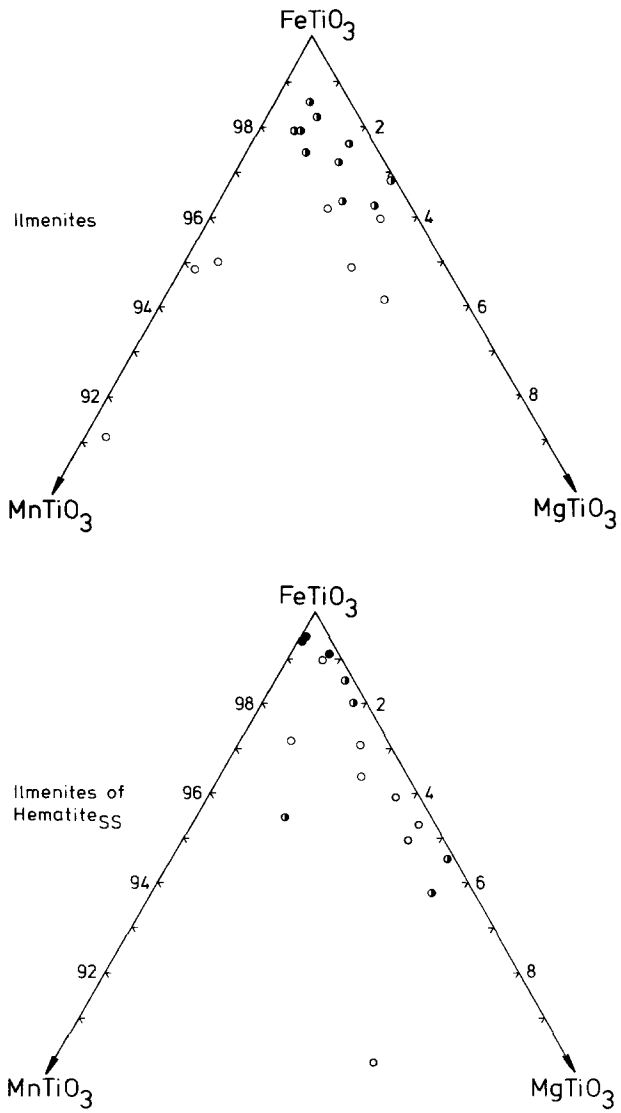

Fig. 8. Composition of ilmenite host crystals (*upper diagram*) and ilmenite exsolution lamellae of hematite solid solutions (*lower diagram*) in terms of the components $FeTiO_3$, $MnTiO_3$ and $MgTiO_3$. Symbols: open circles – ilmenites of eclogites and glaucophane schists; half-filled circles – ilmenites of amphibolitic metabasites; filled circles – ilmenites of prasinites

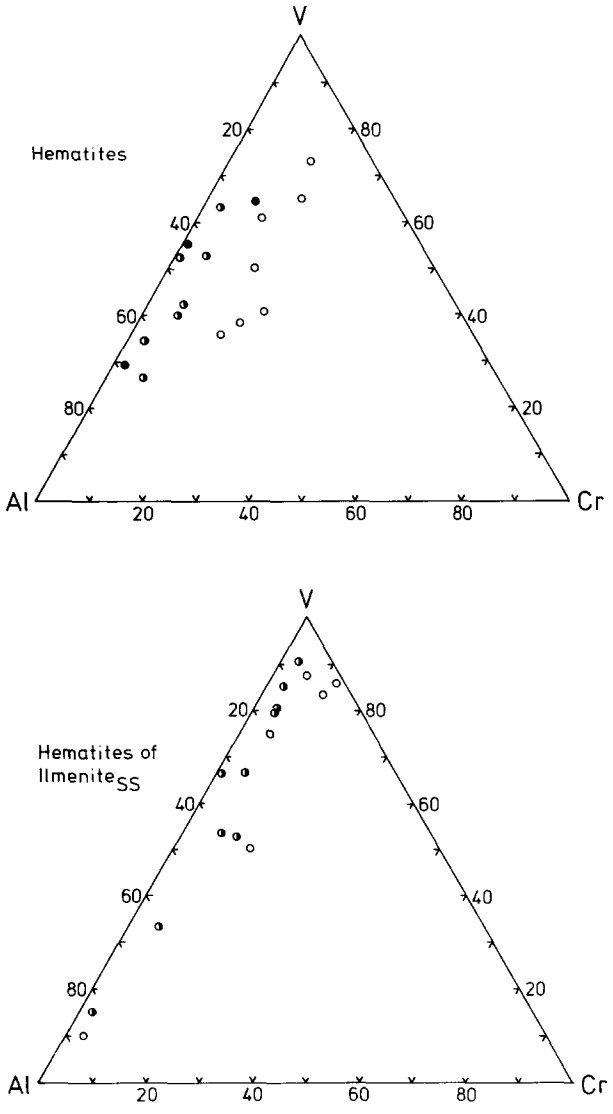

Fig. 9. Minor element composition of hematite host crystals (*upper diagram*) and hematite exsolution lamellae of ilmenite solid solutions (*lower diagram*) in terms of *V*, *Al*, and *Cr*. Symbols: *open circles* – hematites of eclogites and glaucophane schists; *half-filled circles* – hematites of amphibolitic metabasites; *filled circles* – hematites of prasinites

Neumann 1974; Himmelberg and Ford 1977). As a result, variation from ideal hematite chemistry is chiefly confined to the elements V, Al, and Cr (Fig. 9). The hematites show considerable variation in Al and V contents, at relatively low Cr values. However, relatively Cr-rich hematites occur in amphibolitic eclogites, which are Cr-rich rocks. The hematite present in the hemo-ilmenite intergrowths is generally poor in Cr, and the concentrations of V as well as Al are more variable than those of the hematite host crystals. Nevertheless, there is a distinct trend towards high V contents.

Rutile is to a large extent chemically homogeneous (Table 5). Wet chemical analyses of rutiles from glaucophane schists and related rocks (Makanjuola and Howie 1972) indicate that iron occurs in the ferrous state and that Fe^{2+} and Mn^{2+} substitute for Ti^{4+}.

The FeO values for the core and rim areas of the grains vary less than 10% relative. Elemental inhomogeneities are only found in eclogites and glaucophane schists, where rutile inclusions in garnet have a higher average FeO content of 1.2% than the rutile of the matrix (0.7 wt.% FeO). Furthermore, the Nb-content of the rutile relics is slightly higher than that of the rutile of the matrix. This suggests that these compositional differences are the result of a retrogressive depletion of Fe and Nb.

Discussion

Textures and minor element distribution

An analysis of the subsolidus relationships in the system $FeO-Fe_2O_3-TiO_2$ is only meaningful if metamorphic equilibrium was attained. This is particularly true when

Table 4. Microprobe analyses of rhombohedral Fe–Ti phases and molecular proportions

Rock type	Prasinites			Amphibolitic basites												
Sample	54b	50b	49a	44	44	43	42	42	41	40	39	39	38	37	36	35
Two-phase grain	I-H[c]	I-H	I-H	H-I[d]	I-H	H-I	H-I	I-H	H-I	I-H	I-H	H-I	H-I	H-I	I-H	H-I
N[a]	3	4	4	3	5	3	3	3	4	4	5	3	3	5	4	3
SiO_2	0.00	0.00	0.00	0.00	0.00	0.00	0.00	0.00	0.00	0.00	0.00	0.00	0.00	0.00	0.00	0.00
TiO_2	0.33	7.56	8.73	47.12	10.95	47.38	48.30	17.38	46.15	14.36	10.77	48.01	48.72	46.97	15.80	47.65
Al_2O_3	0.47	0.15	0.20	0.54	0.13	0.07	0.00	0.34	0.14	0.17	0.22	0.01	0.14	0.09	0.18	1.35
Cr_2O_3	0.02	0.07	0.01	0.03	0.01	0.01	0.02	0.28	0.04	0.03	0.05	0.02	0.05	0.03	0.02	0.03
V_2O_3	0.30	0.51	0.35	0.15	0.21	0.19	0.14	0.42	0.95	0.50	0.41	0.15	1.02	0.33	0.09	0.13
FeO[b]	87.99	82.27	82.36	48.44	83.11	48.50	48.72	76.97	50.68	76.94	79.49	48.78	48.63	48.38	80.44	48.35
MnO	0.02	0.04	0.04	0.01	0.01	0.33	0.62	0.21	0.51	0.02	0.01	0.66	0.34	0.57	0.43	0.28
MgO	0.18	0.00	0.00	0.75	0.33	0.24	0.28	0.46	0.19	0.14	0.08	0.23	0.16	0.16	0.15	0.74
NiO	0.02	0.00	0.00	0.01	0.00	0.01	0.02	0.02	0.06	0.01	0.01	0.02	0.06	0.00	0.01	0.00
Total	89.33	90.60	91.69	97.05	94.75	96.73	98.10	96.08	98.72	92.17	91.04	97.88	99.12	96.53	97.12	98.53
Ilmenite (mol.%)	0.72	16.14	18.40	91.52	22.25	92.88	93.35	34.62	88.73	29.95	22.81	93.03	93.27	92.32	30.64	90.88
$(Fe,Ni)TiO_3$	99.12	99.47	99.54	96.86	94.59	98.23	97.43	97.59	97.97	98.12	98.60	97.53	98.57	97.98	95.53	96.31
$MnTiO_3$	0.05	0.53	0.46	0.02	0.09	0.78	1.43	0.50	1.23	0.14	0.09	1.53	0.78	1.35	2.77	0.65
$MgTiO_3$	0.83	0.00	0.00	3.12	5.32	0.99	1.14	1.91	0.80	1.74	1.31	0.94	0.65	0.67	1.70	3.04
Hematite (mol.%)																
$(Fe, Al, V, Cr)_2O_3$	99.28	83.86	81.60	8.48	77.75	7.12	6.65	65.38	11.27	70.05	77.19	6.97	6.73	7.68	69.36	9.12

Rock type	Amphibolitic basites					Eclogites and glaucophane schists											
Sample	34	34	33	33	32	31	31	24	23	22	22	21	20	19	18	17	17
Two-phase grain	H-I	I-H	I-H	H-I	H-I	I-H	H-I	I-H	I-H	I-H	H-I	H-I	H-I	I-H	I-H	I-H	H-I
N[a]	3	4	5	6	3	3	3	3	4	6	3	3	3	3	3	3	4
SiO_2	0.00	0.00	0.00	0.00	0.00	0.00	0.00	0.00	0.00	0.00	0.00	0.00	0.00	0.00	0.00	0.00	0.00
TiO_2	46.18	12.50	16.80	47.82	50.34	17.53	46.76	12.18	14.71	17.03	47.15	51.04	50.19	12.48	17.14	17.26	49.54
Al_2O_3	0.19	0.24	0.05	0.04	0.09	0.20	0.14	0.13	0.28	0.26	0.10	0.08	0.02	0.25	0.07	0.17	0.01
Cr_2O_3	0.06	0.04	0.11	0.03	0.03	0.14	0.04	0.11	0.14	0.40	0.03	0.05	0.02	0.04	0.10	0.13	0.04
V_2O_3	0.36	0.30	0.45	0.69	0.85	0.45	0.75	0.21	0.30	0.25	0.19	0.17	0.33	0.28	0.34	0.60	0.36
FeO[b]	51.16	76.87	77.01	48.03	45.80	77.51	49.84	80.86	77.83	76.48	49.62	43.95	45.52	77.16	74.15	73.23	46.75
MnO	0.52	0.10	0.29	1.87	2.21	0.08	0.29	0.03	0.05	0.10	0.64	3.86	0.73	0.10	0.05	0.63	0.82
MgO	0.56	0.38	0.09	0.15	0.06	0.23	0.79	0.30	0.30	0.41	1.03	0.10	0.55	0.19	0.06	0.59	0.83
NiO	0.02	0.00	0.01	0.03	0.01	0.01	0.04	0.01	0.02	0.02	0.04	0.02	0.02	0.02	0.01	0.03	0.02
Total	99.05	90.43	94.81	98.66	99.39	96.15	98.65	93.83	93.63	94.95	98.80	99.27	97.38	90.52	91.92	92.64	98.37
Ilmenite (mol.%)	88.20	57.21	34.04	92.00	96.15	34.97	89.52	24.97	30.15	34.35	89.95	97.52	97.47	26.51	35.82	35.62	95.06
$(Fe,Ni)TiO_3$	96.38	93.78	97.27	95.02	94.84	97.16	96.01	95.38	96.00	95.06	94.18	91.12	96.21	96.48	99.07	90.09	94.85
$MnTiO_3$	1.25	0.81	1.77	4.36	4.92	0.47	0.69	0.25	0.35	0.60	1.51	8.49	1.63	0.81	0.30	3.74	1.85
$MgTiO_3$	2.37	5.41	0.96	0.62	0.24	2.37	3.30	4.37	3.65	4.34	4.31	0.39	2.16	2.71	0.63	6.17	3.30
Hematite (mol.%)																	
$(Fe,Al,V,Cr)_2O_3$	11.80	73.46	65.96	8.00	3.85	65.03	10.48	75.03	69.85	65.65	10.05	2.48	2.53	73.49	64.18	64.38	4.94

[a] Number of analyzed mineral phases
[b] Total iron as FeO
[c] I-H = ilmeno-hematite
[d] H-I = hemo-ilmenite; average chemical analyses, molecular ilmenite of the rhombohedral oxide phases and its composition in terms of $(Fe,Ni,Ca)TiO_3$, $MnTiO_3$, $MgTiO_3$. Maximum error for the ilmenite components: ±1.7 mol.% $(Fe,Ni,Ca)TiO_3$, 0.12 mol.% $MnTiO_3$ and 0.09 mol.% $MgTiO_3$ (host crystals) and ±0.35 mol.% $(Fe,Ni,Ca)TiO_3$ (exsolved phase in hematite). The hematite host crystals as well as the exsolved phase in ilmenite are calculated in mol.% $(Fe,Al,V,Cr)_2O_3$. The maximum error amounts to ±0.89 mol.% (host crystals) and 0.53 mol.% (exsolved hematite)

thermodynamic models are used to calculate equilibrium temperatures and oxygen fugacities on the basis of Fe–Ti oxide compositions. Silicate assemblages, especially those of the eclogitic metabasites, exhibit marked disequilibria (Miller 1977; Spiering 1979). To trace back the complex metamorphic history the occurrence of mineral relics, reaction textures and diaphthoritic minerals are important indicators.

The sequence of exsolution and reaction textures described in the section on opaque mineral assemblages dem-

Table 5. Average chemical composition of rutile

Rock	Prasinites	Amphibolites	Eclogites and glaucophane schists	
n	2	4	3	
			a	b
SiO_2	0.09±0.02	0.26±0.03	0.10±0.04	0.07±0.01
Al_2O_3	0.01±0.01	0.07±0.03	0.03±0.03	0.04±0.03
CaO	0.78±0.21	0.27±0.22	0.47±0.18	0.29±0.02
TiO_2	98.11±0.52	98.51±0.46	98.73±0.49	98.54±0.33
FeO[a]	1.00±0.10	0.89±0.20	0.68±0.06	1.22±0.10
MnO	0.01±0.01	0.01±0.01	0.00	0.02±0.01
Nb_2O_5	<0.01	<0.01	0.03±0.01	0.06±0.02
Ta_2O_5	<0.01	<0.01	<0.01	<0.01

a: composition of matrix rutile
b: composition of "armoured" relictic rutile
n: number of analyzed samples

[a] Total iron as FeO

onstrates progressive chemical adjustment of the Fe–Ti oxides to decreasing $P-T$ conditions during the late stages of alpine metamorphism. Opaque oxide assemblages related to the eoalpine high pressure metamorphic stage have thereby been largely obliterated. In eclogites rutile, ilmenite and magnetite of this stage have been preserved as armoured relics in the cores of garnet and kyanite idioblasts. These rutiles show a much higher Fe content than those present in the matrix. Relict opaque minerals in the metabasites of the Glockner nappe consist of rounded, hematite-free ilmenites or, more commonly, are represented by oxidized ilmeno-hematite in coronar textures. These oxides are also enclosed by fine-grained magnetite idioblasts. Late magnetite which was formed through the retrograde break-down of garnet has a very low Ti content as compared with an older magnetite generation containing a low but distinct ulvöspinel component. Late hematite is clearly distinguishable from ilmeno-hematite of a higher temperature stage because of its mineral textures, chemical homogeneity, as well as near absence of inclusions and exsolution features.

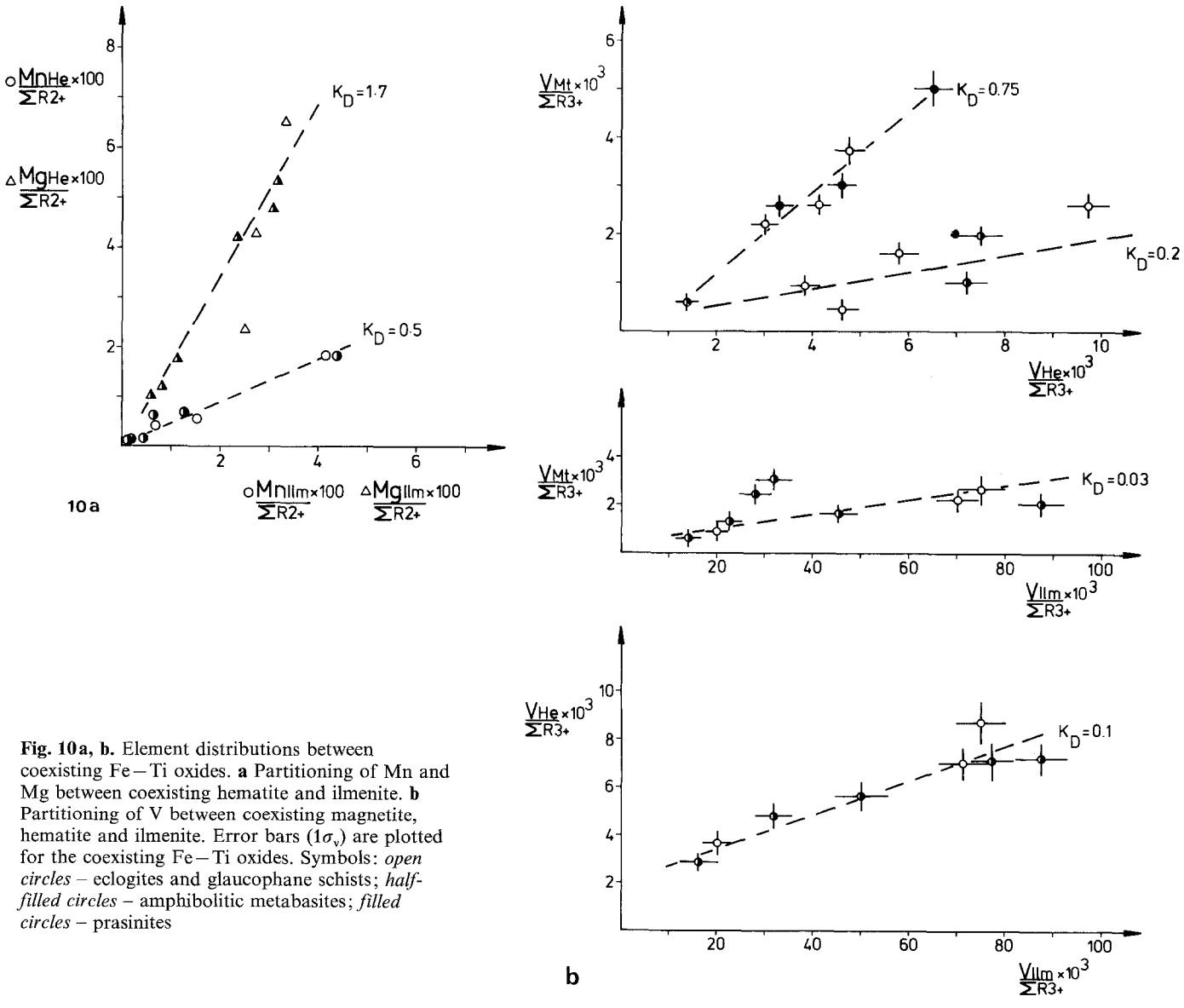

Fig. 10a, b. Element distributions between coexisting Fe–Ti oxides. **a** Partitioning of Mn and Mg between coexisting hematite and ilmenite. **b** Partitioning of V between coexisting magnetite, hematite and ilmenite. Error bars ($1\sigma_v$) are plotted for the coexisting Fe–Ti oxides. Symbols: *open circles* – eclogites and glaucophane schists; *half-filled circles* – amphibolitic metabasites; *filled circles* – prasinites

An important criterion to prove metamorphic equilibrium is the detection of regular partitioning of minor elements between coexisting minerals. The well defined patterns found for the distribution of Mn and Mg between coexisting Fe–Ti phases demonstrate chemical equilibration and considerable element fractionation (Fig. 10a). Mn is enriched in the ilmenite solid solution ($K_D = Mn^{he}/Mn^{ilm} = 0.5$), whereas Mg with the exception of one sample has a higher concentration in the ilmenite component of the hematite solid solution ($K_D = 1.7$). The ilmenite-hematite pairs of amphibolitic and eclogitic rocks clearly plot on the same distribution curve. No data are available for the prasinites. The Mn-distribution coefficient for coexisting magnetite-ilmenite pairs ($K_D = Mn^{mt}/Mn^{ilm} \leqq 0.1$) corresponds to those reported by Haapala and Ojanperä (1972).

The good correlations between the V-contents of coexisting magnetite, ilmenite and hematite also indicate a near to complete attainment of equilibrium distributions (Fig. 10b). The distribution of V between coexisting magnetite and hematite shows two trends. The magnetite-hematite pairs of the prasinites and the diaphthoritic eclogites can be related to an average K_D of 0.75. The distribution data for the mineral pairs from the amphibolites and eclogites form a wide band of values with a considerably lower average K_D of approximately 0.2. This indicates, that the V-distribution between the coexisting phases hematite, ilmenite and magnetite is related to temperature and potentially could be used as a geothermometer. Al shows a similar but less pronounced distribution. The cation-distributions between the Fe–Ti oxides in the amphibolitic and weakly altered eclogitic metabasites obviously reflect comparable temperatures of equilibration.

Thermometry and oxygen-barometry of the Fe–Ti oxides

The partitioning data discussed in the previous section indicate that the compositions of the coexisting Fe–Ti phases represent chemical equilibrium. In this case, $T-fO_2$ data can be calculated by means of thermodynamic models, thus elucidating the temperature and stage of equilibration of hematite-ilmenite pairs in the assemblage with magnetite (Buddington and Lindsley 1964; Powell and Powell 1977; Spencer and Lindsley 1981). The model calculations were carried out using the bulk compositions of the complexly exsolved coexisting ilmenite and hematite (original data are obtainable on request from the authors). The temperature data calculated with the Spencer and Lindsley model are higher by 120–150° C than those obtained by applying the calculation method of Powell and Powell (1977), and the oxygen fugacities obtained from the two methods differ by as much as 10^{-6} atm. The $T-fO_2$ data of the oxide parageneses determined after Powell and Powell (1977) scatter around the magnetite/hematite buffer curve for the pure Fe–Ti–O system and sometimes indicate equilibration at even higher oxygen fugacity. In contrast, the $T-fO_2$ data derived from the Spencer and Lindsley model fall into the $T-fO_2$ stability field of the assemblage magnetite + quartz. Since the natural hematites contain Al_2O_3, and V_2O_3 in addition to exsolved ilmenite, the Fe^{3+}-activity will be lowered and the magnetite/hematite equilibrium should shift to lower oxygen fugacities. Therefore the data obtained from the Spencer and Lindsley model are considered to be more reliable.

The calculated buffer curves for the system FeO–Fe_2O_3–TiO_2 (Fig. 11) based on Eugster and Wones (1962) and Huebner and Sato (1970) are only slightly pressure dependent between 4 and 8 kbars. In addition, the experimental studies of Lindh (1972) also show that between 0.5 and 2.0 kbars the pressure dependence of solid solutions in this system is relatively small. Consequently, this variable can be neglected in further considerations.

The model temperatures obtained for the oxide assemblages of this study range between 380 and 620° C (Fig. 11), and the higher values are relatively close to the temperature estimate of 550 ± 50° C derived from the silicate assemblages (Raith et al. 1980). Temperatures and oxygen fugacities indicate, that the ilmenite-hematite pairs of the metabasites equilibrated in a $T-fO_2$ field between the Ni/NiO and Fe_3O_4/Fe_2O_3 buffer curves. A distinct accumulation of the data points is found near the Fe_3O_4/Fe_2O_3 and MnO/Mn_3O_4 buffer curves (Fig. 11). One unique diaphthoritic eclogite sample (22) contains the strongly oxidized assemblage magnetite and ilmeno-hematite. The hemo-ilmenites in this assemblage appear to be armoured relics within ilmeno-hematite and do not coexist with magnetite. Strongly reduced Fe–Ti oxide assemblages that plot in the $T-fO_2$ region between the Ni/NiO and $Fe_2SiO_4/Fe_3O_4/SiO_2$ buffers which were described by Oliver (1978) for amphibolitic and granulitic gneisses have not been found in this set of samples.

Metamorphic subsolidus miscibilities in the natural system ilmenite – hematite

The thermo-barometric data discussed in the previous section can be used to compare the shape and position of the natural ilmenite-hematite solvus with experimental studies of this solvus. The compositions of the rhombohedral phases coexisting with magnetite-ulvöspinel have been studied at temperatures between 300° and 720° C by Carmichael (1961), Kretschmar and McNutt (1971), Matsuoka (1971), Lindh (1972), Lindsley (1973), and Lindsley and Lindh (1974). The experimental difficulties have been critically discussed by these authors, and so far reversible experiments to determine the ilmenite-hematite solvus have not been successful. The solvi from Lindh (1972) and Lindsley (1973) should therefore be treated with caution.

The bulk compositions of coexisting ilmenite and hematite from the metabasites studied here are presented in a T-x diagram (Fig. 12), using the temperature data calculated with the model of Spencer and Lindsley (1981). A comparison of our own data with that of the experimental solvi is restricted to the shape of the miscibility gap and not to the absolute temperature values because of possible errors in the determination of the bulk compositions and the insufficient knowledge of the influence of the minor elements Mg, Al, V, Cr, and Ni on the position of the solvus. In addition, since the $T-fO_2$ data obtained for the natural assemblages depend on the calculation methods and/or models applied, they can only be considered as first approximations.

The compositions of the hematite solid solutions are represented by a curve, the gradient of which corresponds closely to that of the experimentally derived solvus. Only the hematite from sample 34, which clearly shows disequilibrium oxide textures (see discussion above), deviates from the experimental solvus (ca. 5 mol.% ilmenite component). The hematite with 38 mol.% ilmenite component in the

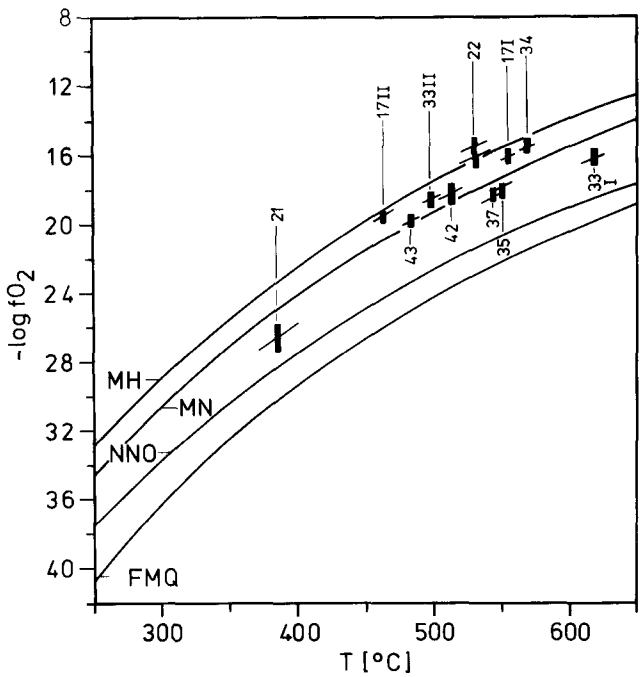

Fig. 11. $T-fO_2$ diagram of ilmenite-hematite pairs coexisting with magnetite. Buffer curves according to Eugster and Wones (1962) and Huebner and Sato (1970): MH – Fe_3O_4/Fe_2O_3, MN – MnO/Mn_3O_4, NNO – Ni/NiO and FMQ – $Fe_2SiO_4/Fe_3O_4/SiO_2$ buffer. $T-fO_2$ data calculated according to Spencer and Lindsley (1981)

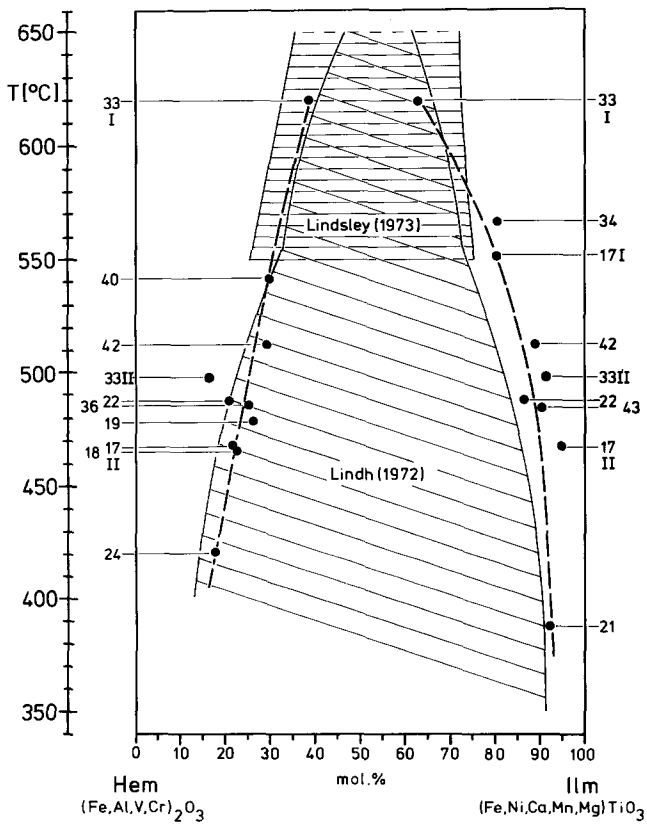

Fig. 12. $T-x$ diagram for the system hematite-ilmenite. The bulk compositions of the hematite and ilmenite phases represented, include the minor elements V, Al, Cr, Mn, Mg and Ni. Solvi according to Lindh (1972) and Lindsley (1973), temperatures for the natural phases calculated after Spencer and Lindsley (1981)

garnet amphibolite 33 is assigned to the maximum temperature assemblage. The ilmeno-hematites coexisting with magnetite in the eclogites 24, 19, 18 are also included in the diagram, although no independent coexisting ilmenite solid solutions were observed. Ilmenite relics in these samples have only been preserved as inclusions in sphene together with hematite-rutile intergrowths. As complex solid solutions the hematites of these assemblages still contain a buffer controlled, temperature dependent ilmenite component, and it is assumed that magnetite participates in the buffer equilibrium.

The solvus of the ilmenite solid solutions resembles the Lindh-solvus, but is shifted to higher ilmenite content. The amphibolite 33 and glaucophanitic eclogite 17 most likely contain two different hemo-ilmenite generations: a high temperature ilmenite generation (I: 620° C/metabasite 33; 550° C/ eclogite 17) and a separate second generation (II: 490° C and 470° C resp.) coexisting with hematite. Ilmenites from the metabasites 21 and 43 occur in the hematite-free assemblages with rutile and magnetite, indicating formation at low fO_2-values within the area defined by the Ni/NiO and MnO/Mn_3O_4 buffers (Fig. 11). The self-buffering effect of this paragenesis in the pure system $FeO-Fe_2O_3-TiO_2$ has been proved by Lindsley and Lindh (1974).

Conclusions

The results of the thermometry and oxygen barometry on the Fe–Ti oxides from the prograde metabasite series imply an unexpectedly large $T-fO_2$ stability field. This suggests that the natural ilmenite-hematite pairs react sensitively to $T-fO_2$ changes by a varying rate of exsolution in the respective rhombohedral phases. Oxides in the amphibolitic and eclogitic rocks probably equilibrated in three different stages:

(1) Re-equilibration at conditions of the low-grade amphibolite facies (< 550° C) leads to the formation of complex intergrowths of ilmenite-hematite solid solutions (e.g. metabasite 17 and 33, cf. Fig. 4a). Suitable mineral sections show typical sandwich-shaped structures built up of ilmenite and hematite layers being bimodally exsolved (Fig. 4c).

(2) With decreasing temperature (500–450° C) the complexly exsolved ilmenite begins to equilibrate following the reaction scheme:

$$\underset{(4FeTiO_3+2Fe_2O_3)}{\text{hemo-ilmenite}_1} \rightarrow \underset{(3FeTiO_3+Fe_2O_3)}{\text{ferrianilmenite}_2}$$

$$+\ \underset{Fe_3O_4}{\text{magnetite}} + \underset{TiO_2}{\text{rutile}}$$

This decomposition runs at constant oxygen fugacities (cf. metabasite 33I/33II and 17I/17II, Fig. 11) and corresponds to a low-grade oxidation of the primary ilmenite. Similarly, the coexisting ilmeno-hematite$_1$ is subjected to a "refining" process, in the course of which lath-shaped rutile and magnetite component are formed:

$$\underset{(4Fe_2O_3+2FeTiO_3)}{\text{ilmeno-hematite}_1} \rightarrow \underset{(3Fe_2O_3+FeTiO_3)}{\text{titanhematite}_2}$$

$$+\ \underset{TiO_2}{\text{rutile}} + \underset{Fe_3O_4}{\text{magnetite.}}$$

(3) At conditions of the lower greenschist facies (<450° C) metamorphic disequilibria are commonly observed, as e.g. hemo-ilmenite or ilmeno-hematite relics within younger sphene overgrowths (eclogite 20). Retrograde alteration of the eclogitic and medium-grade metabasites leads to renewed equilibration. Under oxidizing conditions assemblages that are composed of idiomorphic magnetite in contact with titanhematite and hematite-rutile intergrowths (Fig. 4d, diaphthoritic eclogite 19) are formed, suggesting the following schematic reaction:

$$\underset{(3FeTiO_3+Fe_2O_3)}{\text{ferrianilmenite}_2} + \underset{1/2O_2}{\text{oxygen}} \rightarrow \underset{Fe_3O_4}{\text{magnetite}} + \underset{Fe_2O_3}{\text{hematite}} + \underset{3TiO_2}{\text{rutile}}\,.$$

Intense diaphthoresis of the prasinitic rocks gives rise to hematite-rutile intergrowths, which in part replace ilmenite by the reaction:

$$\underset{(3FeTiO_3+Fe_2O_3)}{\text{ferrianilmenite}_2} + \underset{3/4O_2}{\text{oxygen}} \rightarrow \text{hematite-rutile pseudomorphs}\,.$$
$$2^1/_2Fe_2O_3+3TiO_2$$

This low-grade oxidation leads to the final refinement of titanhematite$_2$ through exsolution of minor and minute lamellae of rutile according to the reaction:

$$\underset{(3Fe_2O_3+FeTiO_3)}{\text{titanhematite}_2} + 1/4O_2 \rightarrow \underset{3^1/_2Fe_2O_3}{\text{hematite}} + \underset{TiO_2}{\text{rutile}}\,.$$

Acknowledgements. We thank J. Schumacher (Kiel), R.A. Yund (Providence), and the reviewers for helpful discussions and the critical review of the manuscript. K. German and W.-D. Bock (Berlin) are thanked for their help and advice with the techniques of Videoplan planimetric analysis. Assistance by E. Siegmann (ARL-SEMQ microprobe) is gratefully acknowledged. The field work was supported by grants from the Deutsche Forschungsgemeinschaft.

References

Abdullah MI, Atherton MP (1964) The thermometric significance of magnetite in low-grade metamorphic rocks. Am J Sci 262:904–917

Abraham K, Hörmann PK, Raith M (1974) Progressive metamorphism of basic rocks from the southern Hohe Tauern area, Tyrol (Austria). Neues Jahrb Mineral Abh 122:1–35

Anderson AT (1968) The oxygen fugacity of alkaline basalt and related magmas, Tristan da Cunha. Am J Sci 266:704–727

Annersten H (1968) A mineral chemical study of a metamorphosed iron formation in northern Sweden. Lithos 1:374–397

Bence AA, Albee AL (1968) Empirical correction factors for the electron microanalysis of silicates and oxides. J Geol 76:382–403

Bowles JFW (1977a) A method of tracing the temperature and oxygen-fugacity histories of complex magnetite-ilmenite grains. Mineral Mag 41:103–109

Bowles JFW (1977b) History of $Fe_3O_4-FeTiO_3$ grains (app.) Mineral Mag 41:16–18

Braun E (1974) Mikrosondenuntersuchungen an metamorphen Gesteinen des Stavanger-Gebietes. DFG-Forschungsber, Clausthal

Buddington AF, Lindsley DA (1964) Iron titanium oxide minerals and synthetic equivalents. J Petrol 5:310–357

Buddington AF, Fahey J, Vlisidis A (1963) Degree of Oxidation of Adirondack Iron Oxide and Iron-Titanium Oxide Minerals in Relation to Petrogeny. J Petrol 4:138–169

Carmichael CM (1961) The magnetic properties of ilmenite-hematite crystals. R Soc London Proc A 263:508–530

Carmichael ISE (1967) The iron-titanium oxides of salic volcanic rocks and their associated ferromagnesian silicates. Contrib Mineral Petrol 14:36–64

Chinner GA (1960) Pelitic gneisses with varying ferrous/ferric ratios from Glen Glova, Angus, Scotland. J Petrol 1:178–217

Eugster HP, Wones DR (1962) Stability relations of the ferruginous biotite, Annite. J Petrol 3:82–125

Haapala I, Ojanperä P (1972) Magnetite and ilmenite from some Finnish Rocks. Bull Geol Soc Finland 44:13–20

Himmelberg GR, Ford AB (1977) Iron-titanium oxides of the Dufek intrusion, Antarctica. Am Mineral 62:623–633

Holland TJB (1977) Structural and metamorphic studies of eclogites and associated rocks in the central Tauern region of the eastern Alps. Unpubl Ph.D. thesis, University of Oxford

Holland TJB (1979a) High water activities in the generation of high pressure kyanite eclogites of the Tauern Window, Austria. J Geol 87:1–27

Holland TJB, Richardson SW (1979b) Amphibole zonation in metabasites as a guide to the evolution of metamorphic conditions. Contrib Mineral Petrol 70:143–148

Huebner JS, Sato M (1970) The oxygen fugacity-temperature relationships of manganese oxide and nickel oxide buffers. Am Mineral 55:934–952

Kaiser H (1965) Zum Problem der Nachweisgrenze. Z Analyt Chem B 209:1–18

Kretschmar UH, McNutt RH (1971) A study of the Fe–Ti-oxides in the Whitestone Anorthosite, Dunchurch, Ontario. Can J Earth Sci 8:947–960

Lindh A (1972) A hydrothermal investigation of the system FeO, Fe_2O_3, TiO_2. Lithos 5:325–343

Lindsley DH (1973) Delimitation of the Haematite-Ilmenite Miscibility Gap. Geol Soc Am Bull 84:657–662

Lindsley DH, Lindh A (1974) A hydrothermal investigation of the system $FeO-Fe_2O_3-TiO_2$: A discussion with new data. Lithos 7:65–68

Makanjuola AA, Howie RA (1972) The mineralogy of the glaukophane schists and associated rocks from the Ile de Croix, Brittany, France. Contrib Mineral Petrol 35:83–118

Matsuoka K (1971) Syntheses of iron-titanium oxides under hydrothermal conditions. Bull Chem Soc Jap 44:719–722

Mielke H, Schreyer W (1972) Magnetite-rutile assemblages in metapelites of the Fichtelgebirge, Germany. Earth Planet Sci Lett 16:423–428

Miller C (1974) On the metamorphism of the eclogites and high-grade blueschists from the Penninic terrane of the Tauern Window, Austria. Schweiz Mineral Petrogr Mitt 54:371–384

Miller C (1977) Chemismus und phasenpetrologische Untersuchungen der Gesteine aus der Eklogitzone des Tauernfensters, Österreich. Tschermaks Mineral Petrogr Mitt 24:221–277

Morse SA (1980) Kiglapait Mineralogy II: Fe–Ti-oxide minerals and the activities of oxygen and silica. J Petrol 21:685–719

Neumann ER (1974) The distribution of Mn^{2+} and Fe^{2+} between ilmenites and magnetites in igneous rocks. Am J Sci 274:1074–1088

Oliver GJH (1978) Ilmenite-magnetite geothermometry and oxygen barometry in granulite and amphibolite facies gneisses from Doubtful Sound, Fjordland, New Zealand. Lithos 11:147–153

Powell R, Powell M (1977) Geothermometry and oxygenbarometry using coexisting iron-titanium oxides: a reappraisal. Mineral Mag 41:257–263

Raith M, Hörmann PK, Abraham K (1977) Petrology and metamorphic evolution of the Penninic ophiolites in the Western Tauern Window (Austria). Schweiz Mineral Petrogr Mitt 57:187–232

Raith M, Mehrens C, Thöle W (1980) Gliederung, tektonischer Bau und metamorphe Entwicklung der penninischen Serien im südlichen Venediger Gebiet, Osttirol. Jahrb Geol Bundesanst Wien 123:1–37

Rollison HR (1980) Iron-titanium oxides as an indicator of the role of the fluid phase during the cooling of granites metamorphosed to granulite grade. Mineral Mag 43:623–631

Rucklidge J, Gasparrini EL (1969) Specifications of a computer program for processing electron micro-probe analytical data. Dept. of Geology, University of Toronto, Ontario, Canada

Rumble D III (1973) Fe–Ti oxide minerals from regionally metamorphosed quartzites. Contrib Mineral Petrol 42:181–195

Rumble D III (1976) Oxide Minerals in Metamorphic Rocks. In: Rumble D (ed) Oxide Minerals. Short Course Notes, Vol. 3. Mineralogical Society of America

Schuiling RD, Feenstra A (1980) Geochemical behaviour of vanadium in iron-titanium oxides. Chem Geol 30:143–150

Spencer JK, Lindsley DH (1981) A solution model for coexisting iron-titanium oxides. Am Mineral 66:1189–1201

Spiering B (1979) Petrologische Untersuchungen von Eklogiten und Glaukophanschiefern des südlichen Venediger-Gebietes (Ostalpen, Österreich). Mineral Diplomarb Universität Kiel

Thompson JB (1972) Oxides and sulfides in regional metamorphism of pelitic schists. 24. Int Geol Congr Precamb Geol Sect 10:27–35

Thy P (1982) Titanomagnetite and ilmenite in the Fongen-Hyllingen basic complex, Norway. Lithos 15:1–16

Wass SY (1973) Oxides of low pressure origin from alkali basaltic rocks, southern Highlands, NSW, and their bearing on the petrogenesis of alkali basaltic magmas. J Geol Soc Aust 20:427–447

Westra L (1970) The Role of Fe–Ti oxides in Plurifacial Metamorphism of Alpine Age in the South-eastern Sierra de los Filabres, SE Spain, Academisch Proefschrift Vrije Universiteit de Amsterdam

Whittaker EJW, Muntus R (1970) Ionic Radii for use in geochemistry. Geochim Cosmochim Acta 34:945–956

Received June 1, 1984 / Accepted January 29, 1985